Kinetics of Initial Layer-by-Layer Oxidation of Si(001) Surfaces

Heiji Watanabe, Koichi Kato, Tsuyoshi Uda, Ken Fujita, and Masakazu Ichikawa
Joint Research Center for Atom Technology, Angstrom Technology Partnership (JRCAT-ATP), 1-1-4 Higashi, Tsukuba, Ibaraki 305, Japan

Takaaki Kawamura
Department of Physics, Yamanashi University, 4-4-37 Takeda, Kofu, Yamanashi 400, Japan

Kiyoyuki Terakura
Joint Research Center for Atom Technology, National Institute for Advanced Interdisciplinary Research (JRCAT-NAIR), 1-1-4 Higashi, Tsukuba, Ibaraki 305, Japan
(Received 23 June 1997)

Layer-by-layer oxidation of Si(001) surfaces has been studied by scanning reflection electron microscopy (SREM). The oxidation kinetics of the top and second layers were independently investigated from the change in oxygen Auger peak intensity calibrated from the SREM observation. A barrierless oxidation of the first subsurface layer, as well as oxygen chemisorption onto the top layer, occurs at room temperature. The energy barrier of the second-layer oxidation was found to be 0.3 eV. The initial oxidation kinetics are discussed based on first-principles calculations. [S0031-9007(97)04959-4]

PACS numbers: 81.65.Mq, 61.16.–d, 68.35.–p, 82.65.–i

Oxidation of Si surfaces is important for technological application of electronic devices [1–3]. Although many kinds of surface analyses have been used to study oxygen adsorption kinetics onto Si surfaces [4–9], the oxidation kinetics of subsurface layers, which determine oxide film growth, have not been studied in detail. This is because of the difficulty of experimentally and independently analyzing the oxidation processes of specific subsurface layers. In this Letter we used scanning reflection electron microscopy (SREM [10]) combined with Auger electron and x-ray photoelectron spectroscopy (AES and XPS) to investigate the initial oxidation of Si(001) surfaces. Our combined analysis has a great advantage for observing layer-by-layer oxidation of subsurface layers, as well as the step and terrace configurations buried with oxide layers. We report, for the first time, reaction barriers of the uppermost and second layer oxidations, and discuss our experimental results based on first-principles calculations.

Our experiments were carried out using an ultrahigh-vacuum surface analysis system that performs SREM, AES, and XPS [11]. This system is equipped with a thermal field emission electron gun, a precision energy analyzer (a spherical capacitor analyzer), and a conventional x-ray source (Mg $K\alpha$ excitation). A 30-keV electron beam with a 2-nm diameter was used for the SREM with a low incident angle of about 2° to the surface. The AES measurement could be performed simultaneously by using the electron gun for SREM at an incident angle and detection angle of about 2° and 73° to the sample surface, respectively. The XPS was performed with a 60° takeoff angle with respect to the normal to the surface. A Si(001)-(2×1) surface was prepared by flash heating with a direct current. Oxidation of the surfaces was carried out by introducing molecular oxygen into the analysis chamber. Since the electron gun and the energy analyzer were independently evacuated, the AES measurement could be performed under oxygen pressure on the order of 10^{-6} Torr.

As we previously reported, since SREM images of SiO_2/Si systems are obtained by recording the intensity change in reflection spots from a crystal Si substrate covered with an amorphous oxide layer, the interfacial structure can be observed without the need to remove the SiO_2 overlayer [12–14]. Figures 1(a)–1(d) show SREM images of Si(001) surfaces before and after oxidation. When we used a specular reflection spot, the (1×2) terraces on Si(001)-(2×1) surfaces, which had dimer rows perpendicular to the incident electron beam, showed bright contrast compared to the alternating (2×1) terraces [Fig. 1(a)] [15]. This surface was oxidized under various conditions, and SREM images were recorded at each oxidation step after oxygen evacuation. Figures 1(b)–1(d) are typical results taken from the same area, where we can still observe the terrace contrast. Oxidation conditions of these figures are Fig. 1(b) 3 min of oxidation at room temperature under 2×10^{-6} Torr oxygen gas pressure, Fig. 1(c) 17 min of oxidation at 635 ℃ following 15 min of oxidation at room temperature under 2×10^{-6} Torr, and Fig. 1(d) a further 65 min of oxidation at 700 ℃ under 2×10^{-5} Torr. After oxygen exposure, the (2×1) reflection high-energy electron diffraction (RHEED) pattern disappeared and only (1×1) spots from the substrate remained. Also, in our previous scanning tunneling microscopy study, no ordered structure was recognized on the surface [16]. Note that the contrast of the initial (1×2) and (2×1) terraces was reversed in each oxidation step,

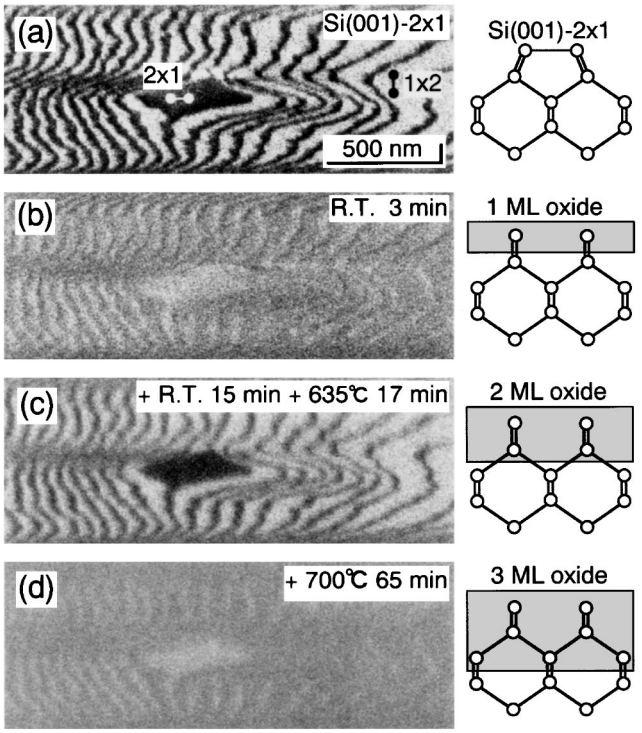

FIG. 1. SREM images of the Si(001) surfaces before and after oxidation. (a) Initial Si(001)-(2 × 1) surface. The dimer direction is shown in the image. Oxidation conditions are shown in the figures. The first contrast reversal (b) corresponds to the oxidation of uppermost dangling bonds and the first subsurface layer as shown in the illustration. (c) and (d) correspond, respectively, to second and third subsurface layer oxidation.

which is consistent with our preliminary results [14], and we also confirmed that the contrast disappeared between these oxidation steps. To clarify the origin of this terrace contrast in the SREM images, we calculated the specular spot intensity from the bulk-terminated Si(001) surface based on the multiple scattering theory of electron diffraction. Details of the calculation method are described elsewhere [17]. Here, we considered two types of bulk-terminated surfaces with uppermost dangling bonds perpendicular (type A) and parallel (type B) to the incident electron beam. The specular spot intensity from the type-B surface was found to be more than 4 times larger than that from the type-A surface under the used glancing angle. By treating the SiO_2/Si system as an interface between the amorphous oxide layer and the bulk-terminated Si surface, we can explain the terrace contrast. Therefore, the periodic reversal of SREM contrast implies layer-by-layer oxidation of the Si(001) surface. It is also notable that the atomic step at the interface did not move laterally and large two-dimensional oxide islands (over 10 nm in diameter) were not observed in any stages, which is consistent with previous TEM [18,19] and our SREM [13] observations of $SiO_2/Si(111)$ interfaces. Thus, we ruled out step-flow oxidation and nucleation of large oxide islands. We consider the most likely layer-by-layer oxidation mechanism to be random nucleation of nanometer-scale oxide islands and subsequent lateral growth [13].

The changes in the terrace contrast in the SREM images were then numerically analyzed and we plotted the difference in spot intensity [$D = I_{1\times2} - I_{2\times1}$, $I_{1\times2}$ and $I_{2\times1}$ are the specular spot intensities at the initial (1 × 2) and (2 × 1) terraces] in Fig. 2(a). This SREM contrast oscillation (SREM oscillation) reveals how many layers were oxidized, just like a RHEED intensity oscillation does during the layer-by-layer film growth [20]. We also performed an AES analysis on the same surface at each oxidation step. Figure 2(b) shows the increase in the oxygen Auger peak intensity (O-*KLL*) normalized by the silicon peak (Si-*LVV*). We can see the staircase increase in the oxygen peak intensity, especially for the first- and second-layer oxidation (oxidation time: 0–18 min and 18–35 min), which also indicates layer-by-layer oxidation. In the Si $2p$ core-level spectrum taken after the final oxidation step [indicated by the XPS arrow in Fig. 2(b)], a chemical shift component from the oxide layer (Si^{4+}) was identified and a small amount of peak intensity from the intermediate oxidation states suggested the presence of an abrupt SiO_2/Si interface [3,21]. Assuming the escape depth of the photoelectron through the oxide layer to be 3.5 nm [13,22], the film thickness was estimated to be 0.63 nm. This estimation means that oxidation of the fourth layer had begun [23], which coincides with the phase of the SREM oscillation [Fig. 2(a)].

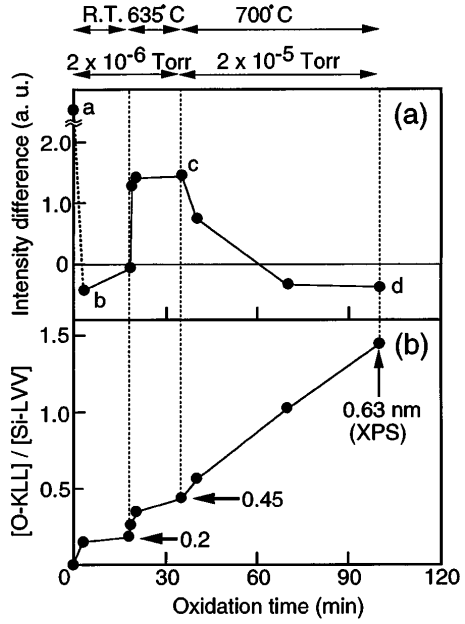

FIG. 2. The change in SREM contrast (a), and the increase in the oxygen Auger peak intensity (b), during oxidation. Oxidation conditions are shown at the top of the figures. The difference in the specular spot intensities between the initial (1 × 2) and (2 × 1) terraces is shown in (a). Oxygen Auger peak intensity normalized by the silicon peak is plotted in (b). At the final oxidation step, the oxide thickness was estimated by XPS to be 0.63 nm. Points "*a*" to "*d*" in (a) correspond to the conditions in Fig. 1.

Comparing the change in the Auger peak intensity with the SREM oscillation [Figs. 2(a) and 2(b)], we can independently investigate the oxidation of a specific layer. Here, we focus our efforts on the first- and second-layer oxidations (see Fig. 3). Note that, since the SREM contrast reversed after oxidation at room temperature for 3 min [Fig. 1(b)], oxygen atom insertion into the back bond, as well as oxygen adsorption onto the uppermost layer, must occur even at low temperatures. The second-layer oxidation requires a much higher temperature. The calibration between the Auger peak intensity and the SREM oscillation shows that the first- and second-layer oxidations were completed at around [O-KLL]/[Si-LVV] = 0.2 and 0.45, respectively [Fig. 2(b)].

To investigate the oxidation kinetics, we measured the time dependence of the oxygen Auger peak intensity during oxidation at temperatures ranging from room temperature to 635 °C. Typical results are shown in Figs. 4(a)–4(d), where Fig. 4(a) and Figs. 4(b)–4(d), respectively, were obtained at 1×10^{-7} and 2×10^{-6} Torr oxygen gas pressures. At room temperature [Fig. 4(a)], the oxygen peak intensities were saturated at about [O-KLL]/[Si-LVV] = 0.2. This indicates the completion of the first-layer oxidation and that it takes much longer for second-layer oxidation to occur under these conditions. According to a recent real-time ultraviolet photoelectron spectroscopy study [7], although it was not clear how many layers were oxidized, the initial oxidation characteristics within a wide temperature range below 600 °C were reported to fit well with Langmuir-type behavior. For the first-layer oxidation, since the slight decrease of the Si-LVV peak can be neglected, the normalized oxygen peak intensity ([O-KLL]/[Si-LVV]) is proportional to the total oxygen amount on the first layer. As shown in Fig. 4(a), our AES data are also consistent with the Langmuir-type reaction. The oxide coverage of the first layer θ_{1st} is given by $\theta_{1st} = 1 - \exp(-R_{1st}t)$, where R_{1st} and t are the initial reaction rate of first-layer oxidation (ML/s) and oxidation time (s). The saturated oxide coverage ($\theta_{1st} = 1$) corresponds to the normalized oxygen peak intensity of [O-KLL]/[Si-LVV] = 0.2. At low temperatures below 200 °C, we could not observe any significant temperature dependence of the initial reaction rate (R_{1st}). This implies a barrierless oxidation of the first subsurface layer (back bond oxidation: case 3 in Fig. 3), as well as oxygen chemisorption onto the top layer (cases 1 and 2). The first-layer oxidation could be completed within 2 min by raising the oxygen gas pressure, and the oxidation rate of the second layer (case 4 in Fig. 3) obviously depends on the substrate temperature, as shown in Figs. 4(b)–4(d). The second-layer oxidation also fits well with the Langmuir-type reaction when the appropriate initial oxidation rate is used for each temperature [$\theta_{2nd} = 1 - \exp(-R_{2nd}t)$, where $\theta_{2nd} = 1$ corresponds to [O-KLL]/[Si-LVV] = 0.25]. The initial sticking probability S_{2nd} [$S_{2nd} = R_{2nd}/F$, where F is oxygen flux (ML/s)] estimated from the curve fitting was plotted based on the Arrhenius equation in Fig. 5. The activation energy for second-layer oxidation was found to be 0.3 eV.

Next, we theoretically investigated the chemisorption of oxygen molecules from the uppermost to the deeper subsurface layers on the Si(001) surface based on

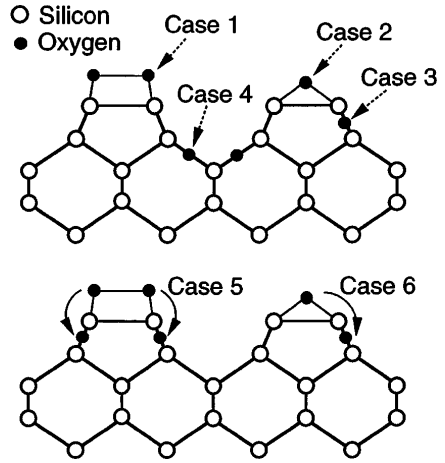

FIG. 3. Schematic illustrations of the initial oxidation. Cases 1 and 2 show chemisorption onto the uppermost layer situated at the top and bridge sites, respectively. Cases 3 and 4 show oxygen atom insertion into the first and second subsurface layers. Cases 5 and 6 show oxygen atom migration from the uppermost layer to the back bond.

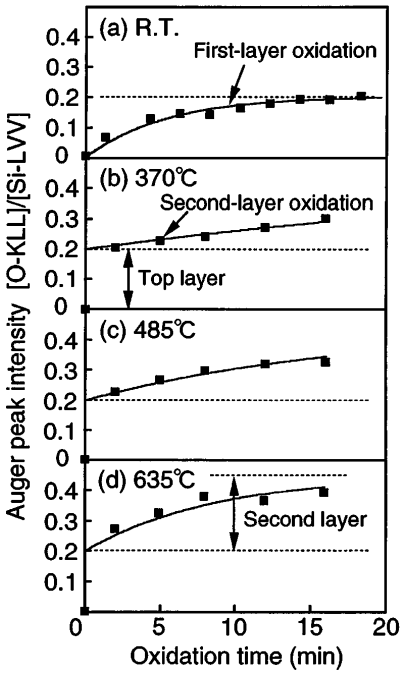

FIG. 4. The normalized oxygen Auger peak intensity as a function of oxidation time at temperatures ranging from room temperature to 635 °C: (a) and (b)–(d) were taken, respectively, at 1×10^{-7} Torr and 2×10^{-6} Torr oxygen gas pressures. The solid lines show the results of curve fitting with an independent Langmuir-type reaction for the first- and second-layer oxidation.

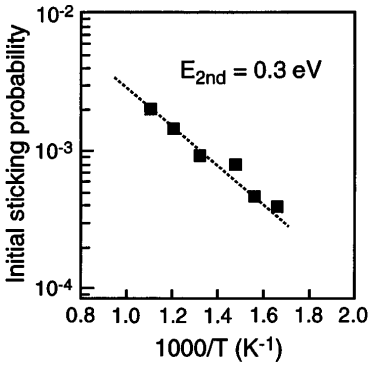

FIG. 5. Arrhenius plots of the initial sticking probability of the second-layer oxidation.

first-principles calculations. Details of the calculations will be described elsewhere [24]. Here, we summarize the calculated results to discuss the initial oxidation mechanism. When the oxygen molecular axis was initially set parallel to the Si(001)-(2 × 1) surface, we found narrow barrierless reaction channels, which resulted in oxygen chemisorption to the top (case 1 in Fig. 3) and bridge sites (case 2). The direct insertion of an oxygen atom into the back bonds of the first (case 3) or second layers (case 4) has a much higher energy barrier of about 1.0 and 2.4 eV, respectively. These calculations imply selective oxygen adsorption onto the top layer. However, our experiments revealed that the first-layer back bond oxidation is also a barrierless reaction. Thus, we considered the migration of oxygen atoms on the uppermost layer to the back bond (cases 5 and 6). Although the energy gains of cases 1 and 2 were, respectively, 2.96 and 5.99 eV, these configurations were found to be metastable and oxygen atoms on the uppermost layer can migrate to the more stable lower-layer back bonds. These calculations explain the rapid and selective oxidation of the first subsurface layer at low temperatures [Fig. 1(b) and Fig. 2(a)]. However, note that the experimentally obtained activation energy of the second-layer oxidation (0.3 eV) is much smaller than the calculated result (2.4 eV, case 4). This is because the oxidized first layer was not considered in the calculations. As previously suggested [25], the mechanism that reduces the reaction barrier for second-layer oxidation could be the effects of the interfacial stress. However, a very complicated model and many assumptions must be introduced to theoretically treat the second-layer oxidation.

In summary, we have investigated the layer-by-layer oxidation kinetics of Si(001) surfaces. Our experiments and calculations have shown that oxygen adsorption onto the uppermost layer and oxygen migration to the back bond are barrierless reactions. The activation energy of the second-layer oxidation was found to be 0.3 eV. The discrepancy between this value and the calculated value suggests that interfacial stress plays a role in oxidation.

We are grateful to Dr. Alexandre Shklyaev of JRCAT for his valuable comments and discussion, and also thank Dr. Akitoshi Ishizaka, Dr. Shinobu Fujita, and Dr. Shigemitsu Maruno for their useful information. This work, supported by NEDO, was performed at JRCAT under the joint research agreement between NAIR and ATP.

[1] P. O. Hahn and M. Henzler, J. Vac. Sci. Technol. A **2**, 574 (1984).
[2] S. M. Goodnick, D. K. Ferry, C. W. Wilmsen, Z. Liliental, D. Fathy, and O. L. Krivanek, Phys. Rev. B **32**, 8171 (1985).
[3] S. Iwata and A. Ishizaka, J. Appl. Phys. **79**, 6653 (1996).
[4] T. Engel, Surf. Sci. Rep. **18**, 91 (1993), and references therein.
[5] M. Tabe, T. T. Chiang, I. Lindau, and W. E. Spicer, Phys. Rev. B **34**, 2706 (1986).
[6] F. Lutz, J. L. Bischoff, L. Kubler, and D. Bolmont, Phys. Rev. B **40**, 10 356 (1989).
[7] Y. Enta, Y. Takegawa, M. Suemitsu, and N. Miyamoto, Appl. Surf. Sci. **100/101**, 449 (1996).
[8] T. Miyake, S. Soeki, H. Kato, T. Nakamura, A. Namiki, H. Kamba, and T. Suzaki, Phys. Rev. B **42**, 11 801 (1990).
[9] A. A. Shklyaev and T. Suzuki, Surf. Sci. **351**, 64 (1996).
[10] M. Ichikawa, Mater. Sci. Rep. **4**, 147 (1989).
[11] H. Watanabe and M. Ichikawa, Rev. Sci. Instrum. **67**, 4185 (1996).
[12] H. Watanabe, K. Fujita, and M. Ichikawa, Appl. Phys. Lett. **70**, 1095 (1997).
[13] H. Watanabe, K. Fujita, and M. Ichikawa, Surf. Sci. **385**, L952 (1997).
[14] S. Fujita, H. Watanabe, S. Maruno, M. Ichikawa, and T. Kawamura, Appl. Phys. Lett. **71**, 885 (1997).
[15] H. Watanabe and M. Ichikawa, Phys. Rev. B **55**, 9699 (1997).
[16] K. Fujita, H. Watanabe, and M. Ichikawa, Appl. Phys. Lett. **70**, 2807 (1997).
[17] T. Kawamura, Surf. Sci. **351**, 129 (1996).
[18] J. M. Gibson and M. Y. Lanzerotti, Nature (London) **340**, 128 (1989).
[19] F. M. Ross and J. M. Gibson, Phys. Rev. Lett. **68**, 1782 (1992).
[20] J. J. Harris and B. A. Joyce, Surf. Sci. **103**, 90 (1981).
[21] M. T. Sieger, D. A. Luh, T. Miller, and T.-C. Chiang, Phys. Rev. Lett. **77**, 2758 (1996).
[22] A. Ishizaka, S. Iwata, and Y. Kamigaki, Surf. Sci. **84**, 355 (1979).
[23] F. Herman and R. V. Kasowski, J. Vac. Sci. Technol. **19**, 395 (1981).
[24] K. Kato, T. Uda, and K. Terakura, Phys. Rev. Lett. (to be published).
[25] For example, B. Leroy, Philos. Mag. B **55**, 159 (1987).